Bulletin of the Seismological Society of America, Vol. 75, No. 3, pp. 737–757, June 1985

EARTHQUAKE FOCAL MECHANISMS IN THE EASTERN TRANSVERSE RANGES AND SAN EMIGDIO MOUNTAINS, SOUTHERN CALIFORNIA AND EVIDENCE FOR A REGIONAL DECOLLEMENT

BY TERRY H. WEBB* AND HIROO KANAMORI

ABSTRACT

Earthquake focal mechanisms obtained from *P*-wave first motions are presented for the Eastern Transverse Ranges and the San Emigdio Mountains in Southern California. The former region shows a predominance of strike-slip faulting whereas Quaternary faults in the region show thrust motion. We suggest that the observed strike-slip mode of deformation cannot continue indefinitely without the occurrence of more thrust faulting. Fault deformation in the San Emigdio Mountains inferred from focal mechanisms is in accord with displacements across Quaternary faults in the area. This study and a search of the literature has yielded 19 mechanisms with shallow-dipping nodal planes. Previous workers have interpreted such mechanisms as evidence for a regional decollement. If such a regional decollement exists, these data give some indication of its regional extent. Slip directions inferred from the focal mechanisms with shallow-dipping nodal planes show some regional consistency, but this pattern cannot be entirely explained with current tectonic models. A comparison of the stress drop of an event having a shallow-dipping nodal plane with an event with steeper planes gave inconclusive results.

INTRODUCTION

Toward understanding the deformation taking place along the San Andreas fault zone in Southern California, we have determined earthquake focal mechanisms in two areas, namely the eastern part of the Transverse Ranges and the San Emigdio Mountains at the western end of the "Big Bend" of the San Andreas fault system (see Figure 1).

The Eastern Transverse Ranges, by which we mean the southeastern region shown in Figure 1, are a unique part of the San Andreas fault system in that no historic large earthquakes have occurred there (Figure 1), although they have in the geologically recent past. This is also a region of considerable fault complexity, with the San Andreas fault branching and intersecting with other fault systems. For these reasons it is important to understand the present pattern of earthquake faulting in this area.

The second area, the San Emigdio Mountains area, is where the 1952 Kern County earthquake ($M_S = 7.7$) initiated (Gutenberg, 1955). We address the problem of whether the present activity follows the same mode of faulting as that determined for the 1952 sequence, and whether it agrees with geological studies of the area (e.g., Davis, 1983).

In studying these two areas, we have found four focal mechanisms that can be interpreted as occurring on very shallow-dipping fault planes. Such mechanisms were first identified by Hadley and Kanamori (1978) and were interpreted as being evidence for a regional decollement. To obtain a more complete picture of the extent of this type of faulting, and to assess its importance with respect to the kinematics of the crust in these regions, we have searched for published mechanisms as well as

* Present address: Geophysics Division, DSIR, P.O. Box 1320, Wellington, New Zealand.

determining fault plane solutions for deeper events (depths greater than 10 km) in the Transverse Ranges. We have also attempted to see if there is any difference in stress drop between these decollement-type events and more typical earthquakes.

In this work, our aim has been to use only well-constrained focal mechanisms. To this end, we have used only the larger well-recorded events ($M_L \geqq 3$ or 3.5) and have avoided the use of composite mechanisms. As a consequence, our distribution of mechanisms is too sparse to resolve small-scale patterns of activity, such as the block rotations studied by Nicholson *et al.* (1983), but we hope to obtain a good constraint on the larger-scale deformation that is presently occurring. The earthquakes we have studied are relatively small and do not necessarily represent the

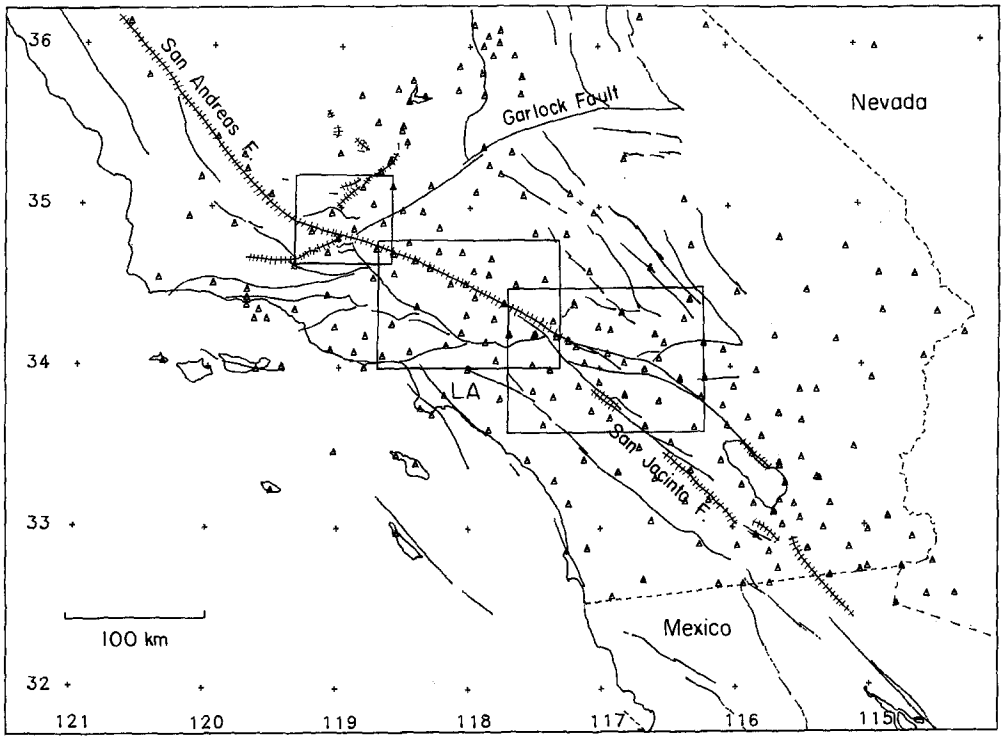

FIG. 1. Map of Southern California showing faults (historic ruptures are *hatched*), stations of the Southern California Seismic Network, and the three areas discussed in the text. The northwestern area is the San Emigdio Mountains, the central one is the Central Transverse Ranges, studied by Pechmann (1983), and the southeastern area is the Eastern Transverse Ranges.

total slip in the region due to the relative motion of the North American and Pacific plates. This will occur in large events on the major faults that are at present quiescent, a fact that is reflected in the present diffuse seismicity throughout the region. However, we believe that this type of study can give a useful insight into the present state of stress in these areas.

EARTHQUAKE MECHANISM DETERMINATION

Earthquake focal mechanisms for the period June 1977 to January 1984 were determined with *P*-wave first motion data from the Southern California Seismic Network. These were supplemented for the period prior to digital recording (before May 1977) by readings from Develocorder film. Station polarities were checked and

corrected by analysis of first motions of suitable teleseisms, local blasts and NTS (Nevada Test Site) blasts kept on file at Caltech. Only clear picks of first motion (i.e., "U" or "D" in the data files) have been used.

All events for which mechanisms were determined were first relocated from *P*-wave arrival times. A four-layered crustal model based on the work of Hadley and Kanamori (1977) was used with thicknesses of 5, 10 and 18 km and corresponding *P*-wave velocities of 5.5, 6.2, and 6.7 km/sec in the layers and 7.8 km/sec in the underlying half-space. Distance weighting was applied to prevent distant stations from influencing the focal depth due to any lateral variations in velocities away from the Transverse Ranges. Formal location errors for more recent data were typically less than 0.5 km for the epicenter and 1.0 km for the depth, with larger uncertainties for earlier data.

Particular attention was paid to determining take-off angles from the focus, since this parameter is the largest source of error in mechanism determinations of this type. Following the method of Pechmann (1983), we plotted reduced travel-time curves at several azimuths for each event to help resolve which paths the picked arrivals followed. The biggest uncertainty in take-off angle occurs at cross-over distances where it is difficult to be sure whether an arrival is directly from the source or is refracted as a head wave. Arrivals from such distances were plotted with small symbols on the first motion diagrams in positions for both up and down-going rays. In hand-fitting the mechanisms, these points could then be considered if they helped to unambiguously determine the solution.

A second major cause of error in take-off angle estimates is incorrect focal depth. When the depth was near a layer boundary, we followed Pechmann's (1983) method of obtaining one solution for each side of the boundary so that the mechanism uncertainty could be determined. Several examples of two solutions for the same event appear in the Appendix (e.g., events 1, 13, and 14). The best-fitting focal depth and least number of polarity violations were used as criteria for selecting one mechanism from each pair. The one used is indicated in the Appendix with an asterisk.

All mechanisms shown in this paper are on equal-area projections of the lower focal hemisphere. The accuracy of the hand-fitted mechanisms was checked by determining the range of *P* and *T* axes corresponding to mechanisms showing the minimum number of stations in error by using the program FOCPLT (Whitcomb, 1973). In a few cases, agreement is not good because the hand-fitted mechanisms have taken account of stations at ambiguous takeoff angles while the computer solutions have not. The present station coverage (Figure 1) means that well-constrained solutions can be obtained for most events larger than magnitude 3.5, and as small as magnitude 3.0 in a few areas, although this was not the case before 1977 when the network was more sparse.

Eastern Transverse Ranges

Figure 2 shows faults mapped for the Eastern Transverse Ranges study area. Some of the relative plate motion in this area is accommodated by slip on the San Jacinto fault, which is probably about half that on the San Andreas itself (Sharp, 1981; Bird and Rosenstock, 1984). A good account of the regional tectonics is given by Diblee (1975) which we summarize briefly here. The San Andreas North Branch is thought, from geological evidence, to be inactive at present, although it has accommodated larger offsets than the South Branch in the past. The South Branch

meets the Banning fault, which shows no Quaternary slip to the west of this junction and is primarily a north-dipping thrust fault (Allen, 1957) until it bends and becomes more strike-slip further to the east. The North Branch, which dips to the northeast (Rasmussen, 1981), is an oblique reverse fault which meets the Mission Creek fault (which shows right-lateral movement) at the Pinto Mountain fault (predominantly left-lateral). In the north of the region, both strike-slip and thrust faulting occur (Jennings, 1975). The surface rupture of the 1857 Fort Tejon earthquake terminated in the area to the northwest of San Bernardino (see, Sieh, 1978 and Figure 1).

Figure 2 also shows recent seismicity for the Eastern Transverse Ranges. Apart from the 1979 Homestead Valley sequence (Hutton *et al.*, 1980; Stein and Lisowski,

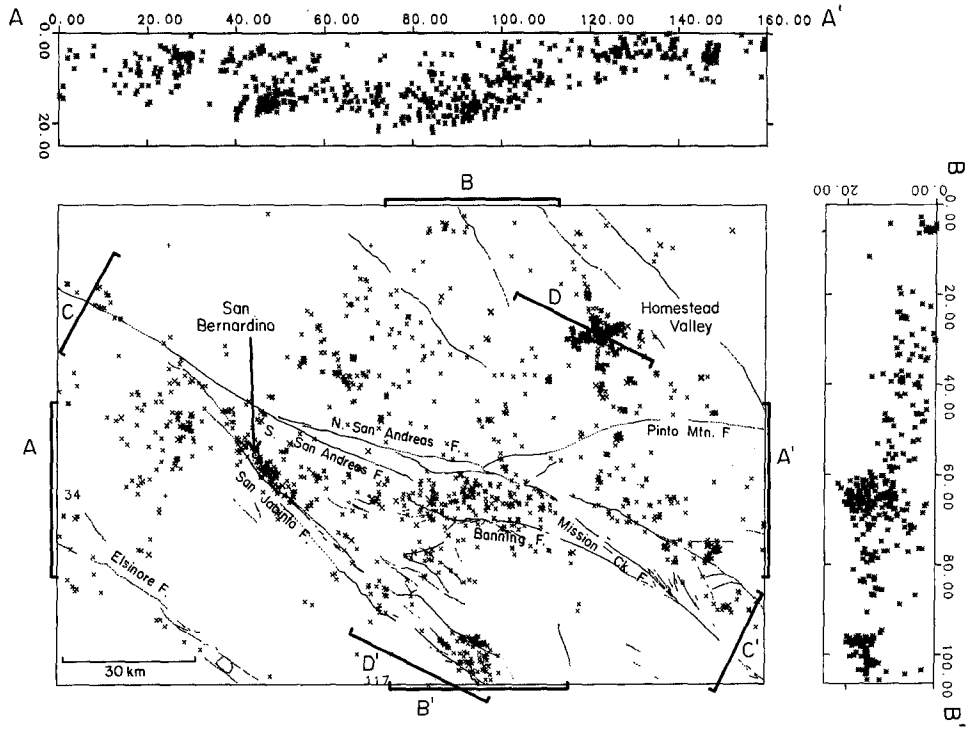

FIG. 2. Map of the Eastern Transverse Ranges study area showing events for the period 1977 to 1983 of magnitude greater than 2 with A quality locations. Small crosses indicate magnitude 2, larger crosses magnitude 3, and asterisks magnitude 4 earthquakes. North-south and east-west depth cross-sections are also shown in 40-km-wide strips.

1983) and seismicity along the San Jacinto fault, which has been studied by Sanders and Kanamori (1984), the seismicity is quite diffuse and does not correlate well with the surface faults. Figures 2 and 3 show depth cross-sections of the seismicity in the area. In the south, activity on the San Jacinto fault is quite distinct. Of more interest to us is the deep activity north of the Banning fault where some of the deepest events in Southern California occur (Corbett and Hearn, 1984). Neither branch of the San Andreas or Banning faults is apparent in the cross-sections; the north-dipping Banning should pass through the intense deep activity, while the northeast-dipping North San Andreas appears to be north of the abrupt change in depth seen in the north-south cross-section. This can best be seen by looking at the

epicentral plot where the sudden increase in activity is clearly south of that fault and does not follow the fault strike, instead having a purely east-west trend. This difference in trend suggests that the observed offset is not due to a systematic mislocation of the events by use of an erroneous velocity model. Green (1983) relocated earthquakes in this area using a master event technique. This does not necessarily remove a systematic mislocation, but the improved relative locations follow the same pattern as described here.

To the north of the Banning fault the seismicity becomes more shallow with activity confined to the upper 10 km. This is clearly seen in the stereo plot in Figure 4.

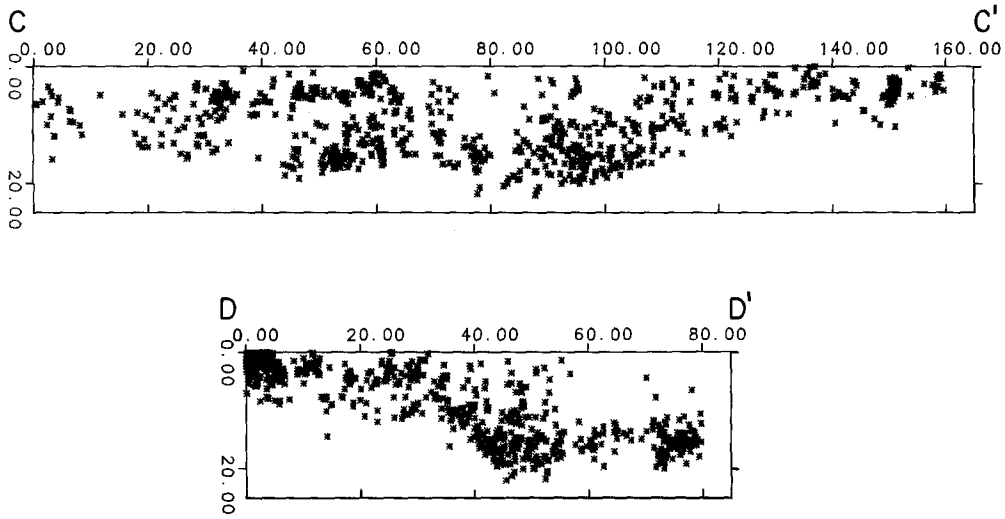

FIG. 3. Two further depth cross-sections for the areas shown in Figure 2.

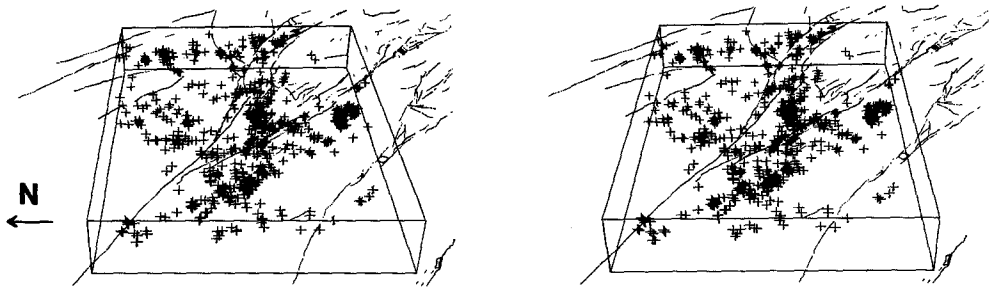

FIG. 4. Stereo plot of earthquakes for the period 1980 to 1983 of magnitude greater than 2 with A quality locations for the Eastern Transverse Ranges area. The depth of the box is 20 km, and the view is from due west.

Figure 5 shows the focal mechanisms obtained for the area divided (arbitrarily) into four subregions. The western region (Figure 5a) has a right-lateral strike-slip event near the San Jacinto fault, three predominantly strike-slip events to the west of the San Andreas, and one normal faulting event close to the San Andreas fault. The three western events could be interpreted as left-lateral on faults near-parallel to the Cucamonga fault (see, Jennings, 1975). The normal faulting near the San

Andreas is likely to be due to stresses created by the junction of the right-lateral San Jacinto and San Andreas fault systems.

In the San Bernardino Mountains to the north (Figure 5b), strike-slip faulting is predominant, and nodal plane directions are consistent between neighbouring events. Three events from a sequence on 13 July 1979 are shown (32, 33 and 34), one of which is distinctly different from the other two. As in the western region there is one purely normal fault event (12), but this is less unusual this far to the north. The northernmost event (30) on the eastern side of Figure 5b is near the

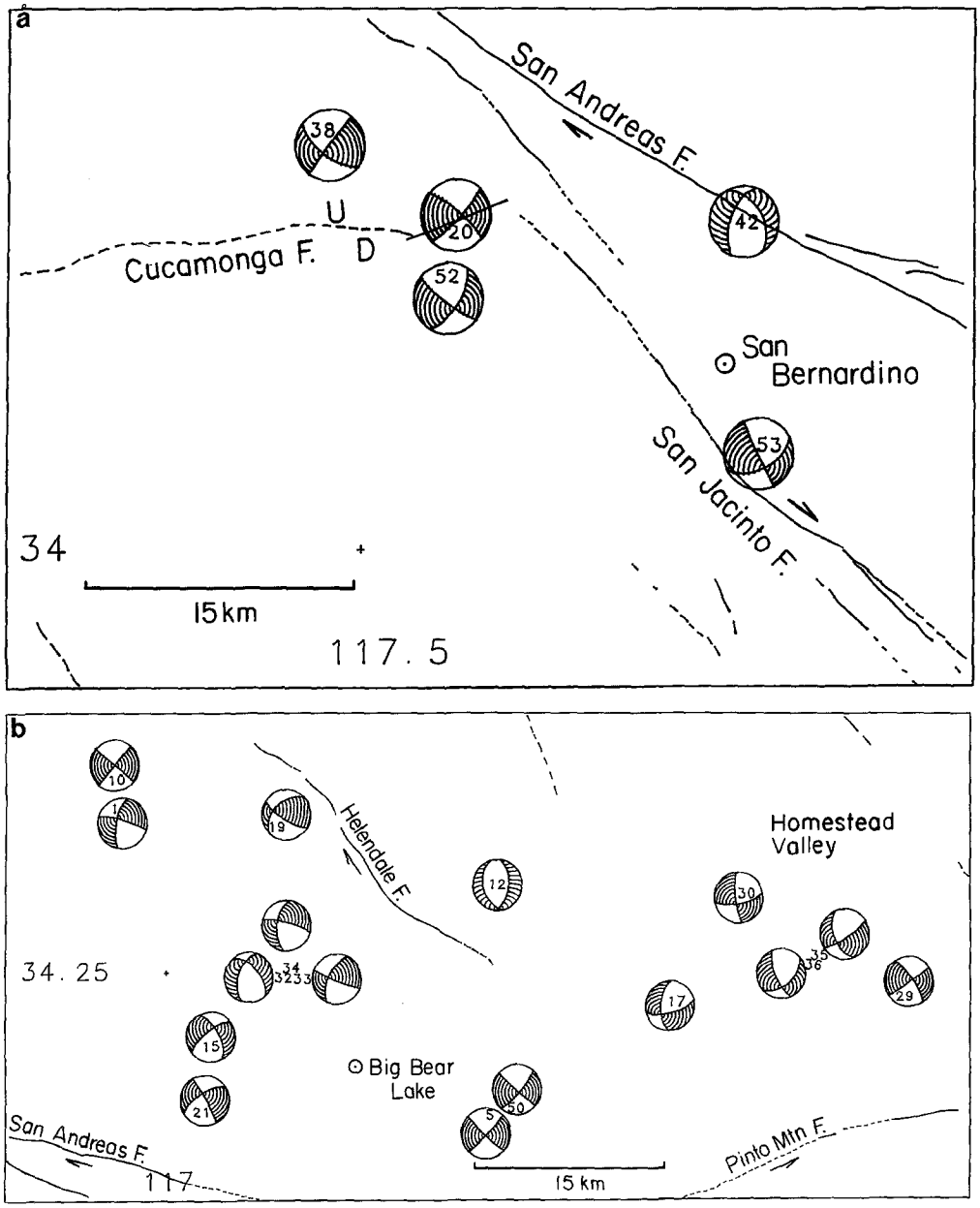

FIG. 5. Maps of focal mechanisms determined for the Eastern Transverse Ranges. All are equal-area projections of the lower focal hemisphere with compressional quadrants *shaded*. The true epicenters are centered at the *middle* of the leftmost digits of the identifying numbers which in turn correspond to the

Homestead Valley sequence and has a very similar mechanism to events in that sequence.

Figure 5c shows the eastern subregion near the Little San Bernardino Mountains where the one event (48) close to the Pinto Mountain fault suggests left-lateral motion along the trend parallel to the Pinto Mountain fault. The other events (3, 4, 31, and 41), which are also largely strike-slip, could also be interpreted as being left-lateral on similar trending faults (one is mapped).

The final subregion (Figure 5d) encompasses the deep activity between the

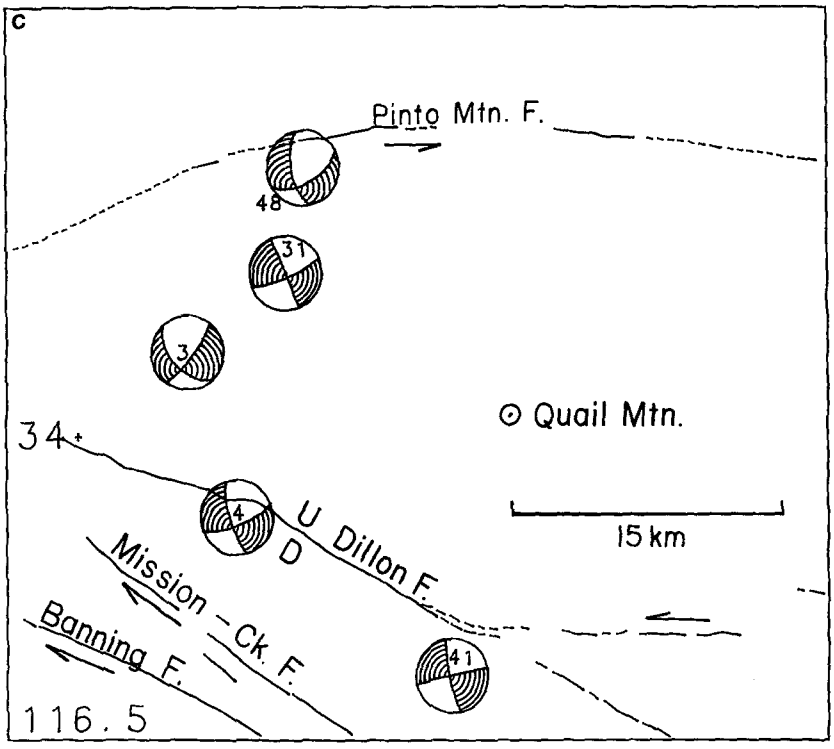

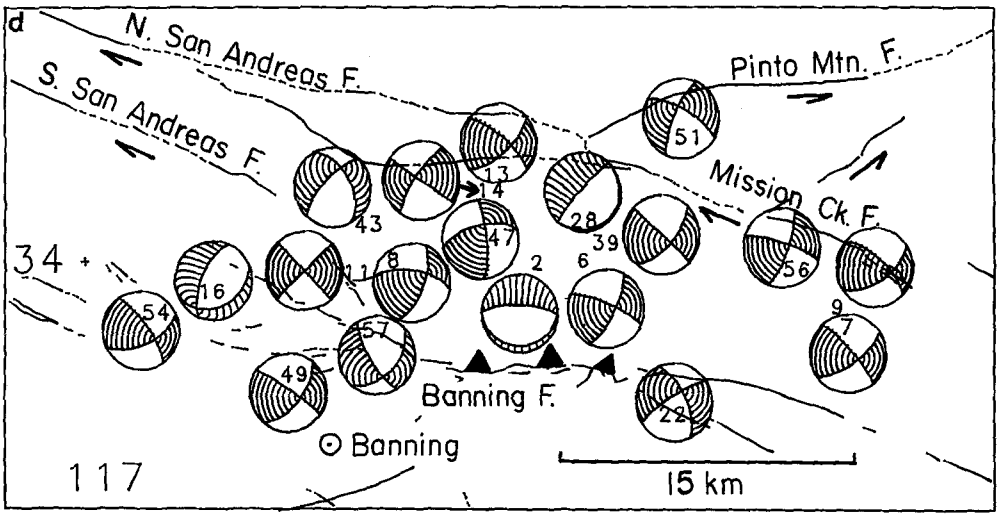

sequence numbers in the Appendix. The figures are of (a) the western, (b) the northern, (c) the eastern, and (d) the central region.

Banning and North San Andreas faults. Two events (2 and 28) have very shallow-dipping nodal planes and are considered in the final section on the evidence for a regional decollement. The other mechanisms are varied oblique thrust and normal faulting as well as strike-slip. The nodal planes do not align with the strike of the major faults.

Discussion of the Eastern Transverse Ranges Mechanisms

The P and T axes for all mechanisms determined in the Eastern Transverse Ranges are shown in Figure 6 along with contours of P and T axis distributions

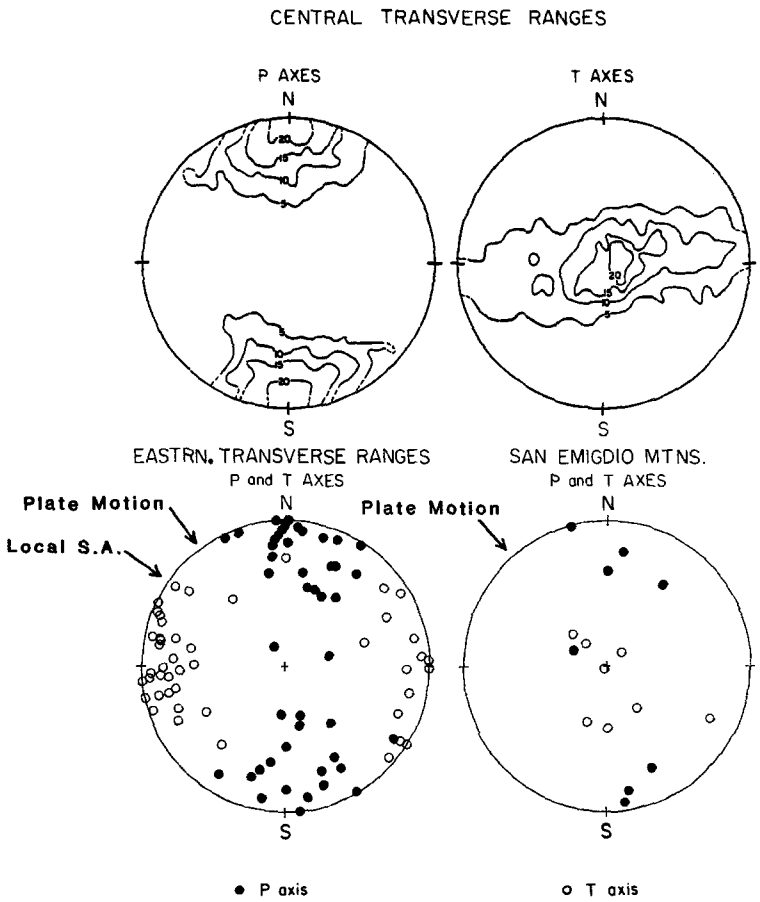

FIG. 6. The *top* diagrams are from Pechmann (1983) and show contours of P and T axis locations from focal mechanisms for earthquakes in the Central Transverse Ranges. Below are equal-area, lower hemisphere plots of the P and T axes (P axes solid circles) for the Eastern Transverse Ranges (*left*) and San Emigdio Mountains (*right*) from focal mechanism solutions. The arrow to the northwest indicates the direction of relative plate motion and the second arrow on the left-hand diagram shows the average local strike of the San Andreas fault in this region.

obtained by Pechmann (1983) for the Central Transverse Ranges. Apart from two normal faulting events, the pattern for our area shows consistent north-south compression which is, on average, horizontal. Similarly there is broad clustering towards near-horizontal east-west extension. Thus, the average mechanism is strike-slip faulting on NE-SW and NW-SE nodal planes. Comparison of this result with the Central Transverse Ranges to the northwest (see Figures 1 and 6) shows very similar N-S compression. However, that area shows T axis directions that are

nearly vertical and are quite distinct from the horizontal ones found here. The average mechanism for that region is thus reverse faulting on E-W trending nodal planes.

Pechmann (1983) argued that his average P and T axis directions reflect the actual tectonic stress field in a statistical sense even though this is not necessarily true for individual earthquakes (McKenzie, 1969). Further, he suggested that the present seismicity is occurring on minor faults of the most favourable orientation to the local stress field. Our results support Pechmann's argument in that the P and T axis directions are clustered and the seismicity is diffuse and is not occurring on the major faults. The P and T axes in Figure 6 should thus represent the directions of maximum and least principal compressive stress respectively with the intermediate principal stress axis being vertical.

Savage (1983) presented strain data from trilateration surveys in Southern California for the period 1973 to 1981. He finds a trend of pure shear strain accumulation locally parallel to the San Andreas fault, with the direction of principal compression rotating through the "Big Bend" region. A model of crustal flow around the "Big Bend" would be consistent with these data. However, pure strike-slip motion on faults oriented obliquely to the relative plate motion can not accommodate the necessary movement. Even if allowance is made for a different local relative plate motion, there must be some crustal shortening in the "Big Bend" region, but this could take place outside the trilateration networks which do not span all of the major thrust faults in the Transverse Ranges area and which would not measure all deformation occurring in thrust earthquakes such as the 1971 San Fernando event. Strain data from triangulation measurements (Savage, 1983), which are made over broader regions than trilateration measurements, show pure shear in agreement with overall plate motion for periods from the 1930's to 1960's. Shear strain accumulation seems to be concentrated near the major faults in Southern California (Savage, 1983) so a possible model for the deformation is one of pure shear strain near and parallel to the major faults with north-south crustal shortening and vertical movement spread over a wider area to accommodate the remaining convergent plate motion. This model agrees with the local geology in that there has been considerable uplift and north-south shortening in the Transverse Ranges, indicated by the existence of thrust faults.

The principal stress directions that we have inferred from focal mechanisms in the Eastern Transverse Ranges agree well with the long-term triangulation data that show pure shear parallel to the relative plate motion. However it is more valid to use the trilateration data of Savage (1983) (discussed above) for comparisons since the Cajon trilateration network covers a similar region to our events and the time period is the same. There is some disagreement with the orientation of the pure shear direction, but this could be due to the strain being concentrated near the major faults while the events for which we have focal mechanisms are more disperse. Pechmann (1983) also found a horizontal north-south principal stress direction for his data. The difference from the principal strain direction may again be due to the occurrence of localised shear stain near the San Andreas fault.

The most obvious difference between earthquake mechanisms in the Transverse Ranges is in the T axis directions, or equivalently, the predominance of thrust faulting in the central area and strike-slip faulting in the eastern one. This difference can be considered as a rotation of the direction of least compressive stress from the vertical in the central area to horizontal in the eastern one.This could be caused by either an increase in the vertical stress or a decrease in the horizontal stress in the

eastern area compared to the central one. There are several possible mechanisms for this. First, a uniform topographic load would increase the vertical stress, and the topography is significantly higher in the eastern region (see, e.g., Oliver, 1980). A second mechanism would be greater isostatic compensation in the eastern region compared with the central area which would also increase the vertical stress. There is evidence for this in the moho depths inferred from *Pn* delay times by Hearn (1983), which show a significantly thicker crust in the eastern area than in the central one.

However, because of the existence of active thrust faults in the Eastern Transverse Ranges, we prefer a model whereby the inferred stress difference is caused by a temporary reduction in the least horizontal compressive stress in the eastern region compared to the central one. The present stress state may be influenced by the pattern of strain accumulation since the last large earthquake in either region. We argue that predominant strike-slip faulting cannot continue indefinitely in the Eastern Transverse Ranges and a change to more thrust faulting at some future time would be expected. Whether this occurs in before, during or after a large earthquake-releasing east-west tension is not known, but continued monitoring of earthquake focal mechanisms in both the Central and Eastern Transverse Ranges may provide an answer.

To conclude this section, we report two null results from our focal mechanism data. If the small earthquakes we have studied do occur on minor faults of the most favourable orientation to the local stress field, we might expect to see a dependence of nodal-plane orientation on earthquake magnitude because there are likely to be fewer larger faults of appropriate orientation. The data set was divided in two according to magnitude, but no significant effect was found.

Vetter and Ryall (1983) found a depth dependence of focal mechanism for earthquakes in the Western Great Basin. No change in the degree of strike-slip as a function of depth could be found in our data for the Eastern Transverse Ranges.

San Emigdio Mountains

Figure 7 shows faults mapped for the San Emigdio Mountains study area. This area includes the "Big Bend" of the San Andreas fault, which ruptured in the 1857 Fort Tejon earthquake. The San Andreas fault is intersected in this region by the left-lateral Big Pine and Garlock faults. The formation of the "Big Bend" is thought to have produced crustal shortening north of the San Andreas which has resulted in the formation of the San Emigdio Mountains (Bohannon and Howell, 1982). These mountains are bounded to the north by the Pleito thrust system. The White Wolf fault shows both thrust and left-lateral movement and last ruptured in the 1952 Kern County earthquake.

Figure 7 also shows recent seismicity in the San Emigdio Mountains. We have plotted the A and B quality catalog locations with a depth key because the distribution of seismicity is too complex to be well presented with cross-sections. As a check of the catalog locations, we plotted A and B quality solutions separately, but no significant difference in the seismicity patterns was noted. The pattern of seismicity is also shown in a stereo plot in Figure 8.

At the northwestern edge of the seismicity is a northeast-trending band of activity, the maximum depth of which increases from 10 km in the southwest to 15 km in the northeast. This activity does not show a clear planar pattern on depth-cross sections or in stereo plots. The 1952 Kern County aftershock distribution also showed a diffuse zone of activity (Cisternas, 1964), although the aftershocks were

not well-located by modern standards. Cisternas interpreted the diffuse activity as occurring on several near-parallel-dipping structures. Shocks occurring within 2 days of the main shock were more concentrated on the inferred fault plane.

Since the recent seismicity lies near the inferred fault plane for the 1952 Kern County earthquake (Stein and Thatcher, 1981) and since both historic aftershocks

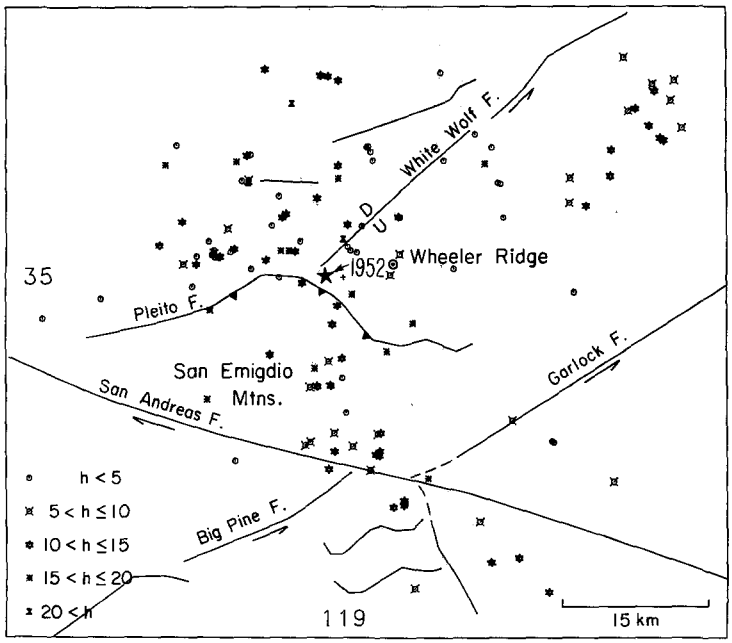

FIG. 7. Map of the San Emigdio Mountains showing A and B quality events for the period 1981 to 1983. Note that each event is represented with a depth key. The large star marks the epicenter of the 1952 (M_S = 7.7) Kern County earthquake.

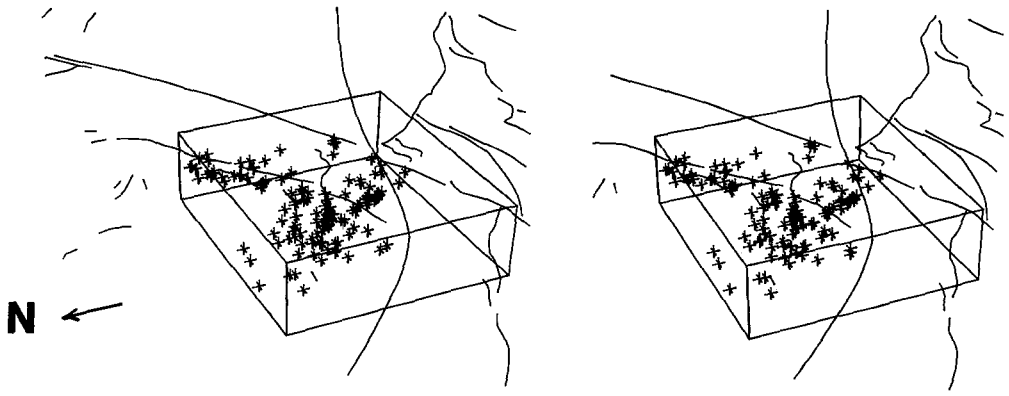

FIG. 8. Stereo plot of A and B quality events for the period 1981 to 1983 for the San Emigdio Mountains region. The box is 20 km deep, and the view is from the WNW.

and recent seismicity are diffuse, we believe that the observed northeasterly band of activity is related to the White Wolf fault zone. This contention could be checked by a systematic relocation of events using either a homogeneous station method (Ansell and Smith, 1977) or master event technique (Johnson and Hadley, 1976) when more data become available.

Figure 7 shows some seismicity near the Pleito fault system, but activity further to the north does not coincide with any mapped fault. However, any existing faults in this area would be covered by sedimentary material.

Another trend of activity runs from near the 1952 rupture point to the southeast and is relatively deep (15 to 20 km). It even appears to cross the San Andreas fault, but again it does not show a planar structure in cross-sections. This activity does not correlate with any feature of the surface geology mapped by Davis (1983), although this is not too surprising considering the depth of the seismicity. It is an unusual feature in that it seems to cross the San Andreas fault, which is a major tectonic boundary. We consider it unlikely to be related to the San Andreas since the strike of that fault is different from the strike of the southeasterly trending seismicity.

In Figure 9, we have plotted all of the reliable focal mechanisms obtained for the region. The time period is more limited than for our first study area because of

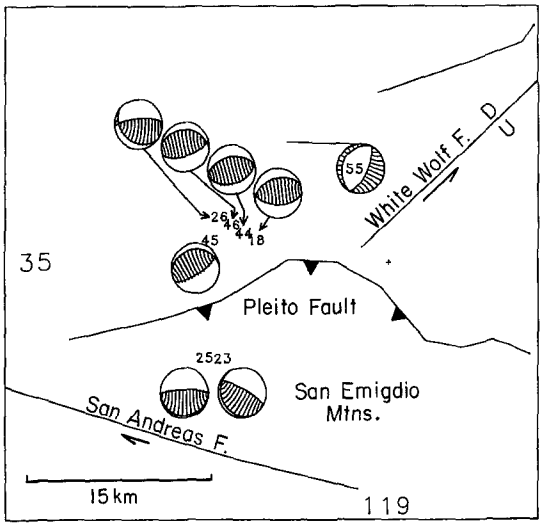

FIG. 9. Maps of focal mechanisms obtained for the San Emigdio Mountains area. Details are the same as for Figure 4.

earlier network sparseness. Five events occur in one group near the 1952 Kern County epicenter, all of which are shallow and predominantly thrusts. Three of these occurred as a part of a sequence, but the other two were at separate times. Their nodal planes are consistent with the orientation of mapped faults in the area. Cross-sections from Davis (1983) show great complexity in this region at the edge of the thrust zone, and the observed mechanisms are in good agreement with those expected from the geology and general north-south compression. The plot of P and T axes (Figure 6) confirms that the average mechanism shows north-south compression and predominant thrusting, apart from the one normal faulting event observed to the northwest. The predominant north-south compression agrees with the pirncipal strain directions for the Los Padres and Tehachapi trilateration networks presented by Savage (1983) and King and Savage (1984), respectively. The normal faulting event was relatively deep (15 km) and may have such a mechanism because of the increased vertical stress at this depth, but it is not too well-constrained, and more data are needed before any conclusion can be drawn about present activity on the White Wolf fault.

The two southernmost events have very shallow-dipping nodal planes. If these are assumed to be the fault planes, they are consistent with movement on a near-horizontal surface with the top block moving to the north. The focal depths are very shallow, but since the nearest station is over 10 km away in each case, any depth within the top 5 km is possible. The existence of shallow-dipping faults within this depth range was inferred from well log data by Davis (1983). These events are discussed further in the next section.

The 1952 Kern County event was most likely an oblique thrust with a significant left-lateral strike-slip component (Kanamori, unpublished data). The lack of any strike-slip component in our mechanisms indicates that they are purely a response to the thrust deformation that created the San Emigdio Mountains, and that shear strains are not being released at this end of the White Wolf fault at present. This would seem to support the observation of Davis (1983) that the San Emigdio Mountains are a pure thrust system, but we find no evidence in our data for or against his contention that this continues through the San Andreas fault. Moreover, the fault model proposed by Bohannon and Howell (1982) for the formation of the "Big Bend" predicts pure thrust faulting for this region.

An attempt was made to determine focal mechanisms for the aftershocks of the Kern County event. This was difficult because of poor focal depth control and sparse coverage of the focal sphere. Composite plots showed great scatter indicating a great variety of faulting behavior, as originally presented by Båth and Richter (1958). As the mechanisms showed clear dependence on assumed focal depth this study was not pursued.

To summarize, some features of seismicity in the San Emigdio Mountains correlate with the inferred fault plane of the 1952 Kern County earthquake, while the southeasterly trend of relatively deep activity is not understood. Thrusting on shallow dipping fault planes agrees with the listric faults mapped by Davis (1983), while pure thrusts on steeper planes further to the north occur in a complex zone of thrusting at the edge of the Wheeler Ridge. No strike-slip activity is observed at present.

Regional Decollement

Hadley and Kanamori (1978) identified two earthquake focal mechanisms that could be interpreted as occurring on shallow-dipping thrust faults in the Central Transverse Ranges. One event was an aftershock of the 1971 San Fernando earthquake, the other was an event 30 km to the southwest. Both occurred near the bottom of the seismogenic zone and were considered to be evidence for a regional decollement. The existence of such a horizontal detachment surface under Southern California has been proposed by several authors [e.g., Anderson (1971); Sibson (1983); Crouch *et al.* (1984)] and is thought to be caused by a change in mineralogical properties with the increased temperatures at mid-crustal depths. Other authors have more recently identified further mechanisms with shallow-dipping nodal planes, and four have been identified in the work presented above. In Figure 10 we have plotted focal mechanisms and slip directions for all of the events showing low angle thrusting that we could find in the literature, as well as other events selected with catalog depths greater than 10 km and a fault plane dipping at less than 25°.

Mechanisms 58 through 61 and 65 are taken from Lee *et al.* (1979), but as the first motion data for individual stations are shown only for one of these events, their reliability cannot be assessed. However, the authors do mention that care was taken in using only well-constrained mechanisms. Mechanisms 66 and 67 are from

Hadley and Kanamori (1978). Numbers 62, 63 and 64 are from Stierman and Ellsworth (1976) and are aftershocks of the 1973 Point Mugu earthquake. The aftershock depth distribution was very flat, suggesting faulting on a horizontal structure. Numbers 68 and 69 are from Corbett and Johnson (1982) and are aftershocks of the 1978 Santa Barbara earthquake. Again, the aftershock distribution was nearly horizontal, and the main shock mechanism was very similar to that at Point Mugu except for a 20° rotation. All of the latter mechanisms should be well-constrained.

The remaining mechanisms in Figure 10 are from this work, four coming from the areas studied in the first sections while the remainder were selected according to the criteria above. The degree of constraint on the dips of the nodal planes can be assessed by examining the size of the P and T axis contours on the mechanisms shown in the Appendix. One source of uncertainty not accounted for is the inadequacy of a horizontally-layered velocity model in calculating take-off angles for rays

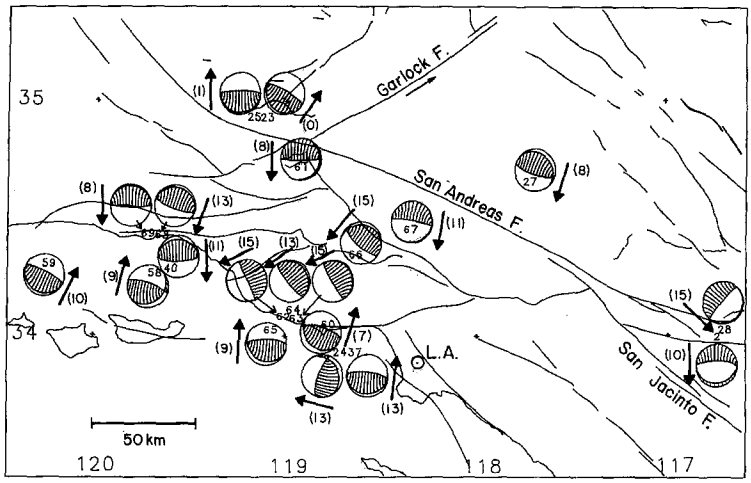

FIG. 10. Map of focal mechanisms for all of the decollement-type events (one nodal plane dipping at less than 25°) in the Transverse Ranges area. Details are the same as for Figure 4 except that arrows mark the direction of the horizontal projection of the slip vectors for the shallow-dipping nodal planes. Figures in parentheses are the respective focal depths. Events are from this work and other sources mentioned in the text.

leaving the source. If the real ray paths were systematically affected by velocity gradients at the base of the brittle crust, all events should show similar distortion. This is not observed.

The two northernmost events discussed previously (23 and 25), suggest that a near-horizontal decollement exists below the San Emigdio Mountains. An important question is whether this structure continues through the San Andreas fault zone, or whether smaller, localized "flakes" exist on either side of the fault. Davis (1983) contends that the structure continues through the fault, eventually joining the horizontal brittle-ductile transition zone. Such a model is illustrated schematically by Figure 11a. Yeats (1981) also proposed the existence of a regional decollement in his flake tectonic model, but in his model the plate boundary at depth is offset from the San Andreas fault that breaks the brittle region (Figure 11b). Mechanism 61 should be very important in this regard, but the depth of this event is unreliable (the nearest station being 25 km away) and thus the mechanism could also be of doubtful reliability. The two events discovered by Hadley and Kanamori (1978) (66

and 67) occurred at the base of the seismogenic zone and their direction of slip suggests that the decollements are local to one side of the San Andreas fault zone, or at least cross it within the ductile layer, as suggested by Yeats (1981). Events to the west of these are consistent with this in that the upper block moves south or southwest relative to the lower one. However, further to the southwest there are six events that show upper block motion ranging from northwest to northeast. They form a lineation nearly parallel to the coast and to the local strike of the San Andreas. These may be occurring on south-dipping faults such as the Oak Ridge fault (Yeats, 1981), and may indicate the existence of a separate decollement with an opposite direction of slip from the one to the northeast. This is depicted schematically in Figure 11c.

In discussing the crustal kinematics, one needs to consider the driving forces that have created the "Big Bend." Both Humphreys and Hager (1984) and Bird and Rosenstock (1984) have presented models that involve aseismic subduction of ductile

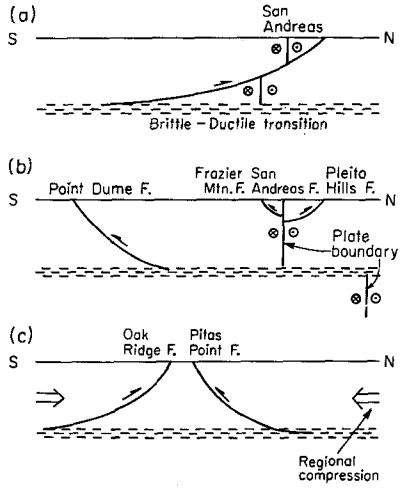

FIG. 11. (a) The tectonic model of Davis (1983) for the San Emigdio Mountains. (b) A schematic figure on the basis of the cross-sections of Yeats (1981) showing the offset of the plate boundary at depth and the regional decollement. (c) Our model for explaining the occurrence of decollement-type events with opposite slip directions parallel to the Southern California coast.

lithospheric material under the Transverse Ranges. The crustal flow model deduced by Bird and Rosenstock (1984) assumes *a priori* that the flow in most areas is equal to the upper mantle flow, thus leaving no flow differential to form a decollement. The horizontal tractions near the base of the lithosphere calculated by Humphreys and Hager (1984) are more relevant, although they choose to apply their basal tractions at a depth greater than the inferred regional decollement, which is at mid-crustal depths. There is broad agreement between their results and our inferred slip directions, but there is no obvious mechanism for the sudden change in slip direction in the southwest, shown by six of our events. However, simple northeast-southwest compression causing crustal shortening would explain the observations.

The direction of slip of the Eastern Transverse Ranges events (with the upper block moving south or southeast) are consistent with those expected, but the lack of mechanisms here makes it difficult to determine the extent of any decollement.

One unusual event is number 27 which lies to the northeast of the San Andreas fault zone and shows southwestward movement of the upper block. This solution is

primarily constrained by one data point. If this is of incorrect polarity, a mechanism with the opposite sense of slip could be obtained. Further study of focal mechanisms in this area to the northeast of the San Andreas fault would be very valuable.

If the events with shallow-dipping nodal planes are occurring on a decollement interface, one might expect that their spectral characteristics would be different from those of other events. This difference could be expected because of the change in mineralogical properties of the rocks in the respective source regions. To test this hypothesis, we attempted to calculate stress drops of event 28 (low-angle normal faulting) and event 39 (predominantly strike-slip) using the initial pulse widths recorded at nearby stations, following the method of Frankel and Kanamori (1983).

For the nondecollement event (39), there were no significant differences in pulse width between it and a calibration event for the seven stations that recorded satisfactory nonnodal arrivals. The decollement event had pulse width differences of 0.03 (50 per cent) and 0.08 (80 per cent) sec at two stations, but none at four other stations. The azimuthal distribution of stations was such as to rule out this being a directivity effect, so these data are inconsistent. If we simply averaged these results in comparing the main events, they would suggest a lower stress drop for the decollement event, but we regard the results as suggestive, but inconclusive.

Conclusions

Focal mechanisms of earthquakes in the Eastern Transverse Ranges show a predominance of strike-slip faulting which we did not expect in light of geological data. In the long-term (on the order of the repeat time of large earthquakes here), we expect that more thrust faulting will occur, either as small events or in a single event, and that the Eastern Transverse Ranges will continue to be uplifted.

Few focal mechanisms could be obtained for the San Emigdio Mountains area, but those that were found indicate pure thrusting at the present time which agrees well with the geology. Some of the seismicity in this area can be interpreted in terms of activity near the White Wolf fault, but we have no explanation for a deep southeasterly trend of activity.

A compilation of focal mechanisms having shallow-dipping nodal planes gives an indication of the regional extent of a possible decollement in the Transverse Ranges region. Inferred slip directions are in broad agreement with the horizontal tractions calculated by Humphreys and Hager (1984), but a reversal of slip direction near the southwestern limit of the observed low-angle mechanisms is unexplained.

Acknowledgments

We wish to thank W. L. Ellsworth of the USGS at Menlo Park for providing replays of FM tapes and Art Frankel for many useful discussions. Ed Corbett, Tom Hearn and Carl Johnson gave assistance in accessing the phase data which was collected by the dedicated Caltech and U.S.G.S. staff. Don Anderson, Art Frankel, Gene Humphreys, Jim Pechmann, Chris Sanders, Steve Wesnousky, and an anonymous reviewer provided useful comments on the manuscript. This study was made while one author (T. H. W.) was on a Study Award from the Department of Scientific and Industrial Research New Zealand at the California Institute of Technology, Pasadena. The research was partly supported by USGS Contract 14-08-0001-21210.

References

Allen, C. R. (1957). San Andreas fault zone in San Gorgonio Pass, Southern California, *Bull. Seism. Soc. Am.* **68**, 315–350.

Anderson, D. L. (1971). The San Andreas fault, *Sci. Am.* **225**, 52–66.

Ansell, J. H. and E. G. C. Smith (1975). Detailed structure of a mantle seismic zone using the homogeneous station method, *Nature* **253**, 518–520.

Båth, M and C. F. Richter (1958). Mechanisms of the aftershocks of the Kern County, California, earthquake of 1952, *Bull. Seism. Soc. Am.* **48,** 133–146.

Bird, P. and K. Piper (1980). Plane-stress finite element models of tectonic flow in Southern California, *Phys. Earth Planet Interiors* **21,** 158–175.

Bird, P. and R. W. Rosenstock (1984). Kinematics of present crust and mantle flow in Southern California (submitted for publication).

Bohannon, R. G. and D. G. Howell (1982). Kinematic evolution of the junction of the San Andreas, Garlock, and Big Pine faults, California, *Geology* **10,** 358–363.

Cisternas, A. (1964). Precision determination of focal depths and epicenters of earthquakes, *Ph.D. Thesis* (Part II), California Institute of Technology, Pasadena, California.

Corbett, E. J. and C. E. Johnson (1982). The Santa Barbara, California, earthquake of 13 August 1978, *Bull. Seism. Soc. Am.* **72,** 2201–2226.

Corbett, E. J. and T. M. Hearn (1984). The depth of the seismic zone in the Transverse Ranges of Southern California (abstract), *Earthquake Notes* **55,** 23.

Crouch, J. K., S. B. Bachman, and J. T. Shay (1984). Post-Miocene compressional tectonics along the central California Margin, in *Tectonics and Sedimentation along the California Margin.* J. K. Crouch and S. B. Bachman, Editors, Pacific Section, S. E. P. M. **38,** 37–54.

Davis, T. L. (1983). Late Cenozoic structure and tectonic history of the western "Big Bend" of the San Andreas fault and adjacent San Emigdio Mountains, *Ph.D. Thesis,* University of California, Santa Barbara, California.

Dibblee, T. W. (1975). Late Quaternary uplift of the San Bernardino mountains on the San Andreas and related faults, *Calif. Div. Mines Geol. Spec. Rept.* **118,** 127–135.

Frankel, A. and H. Kanamori (1983). Determination of rupture duration and stress drop for earthquakes in Southern California, *Bull. Seism. Soc. Am.* **73,** 1527–1551.

Green, S. M. (1983). Seismotectonic study of the San Andreas, Mission Creek, and Banning fault system, *M.Sc. Thesis,* University of California, Los Angeles, California.

Gutenburg, B. (1955). Epicenter and origin time of the main shock on July 21 and travel times of major phases, in *Earthquakes in Kern County, California During 1952,* G. B. Oakeshott, Editor, *Calif. Div. Mines Bull.* **171,** 157–163.

Hadley, D. and H. Kanamori (1977). Seismic structure of the Transverse Ranges, California, *Bull. Geol. Soc. Am.* **88,** 1469–1478.

Hadley, D. and H. Kanamori (1978). Recent seismicity in the San Fernando region and tectonics in the west-central Transverse Ranges, California, *Bull. Seism. Soc. Am.* **68,** 1449–1457.

Hearn T. (1983). *Pn* travel times in Southern California, *J. Geophys. Res.* **89,** 1843–1855.

Humphreys, E. and B. H. Hager (1984). Small-scale convection beneath the Transverse Ranges, Southern California (abstract), *EOS* **65,** 195.

Hutton, L. K., J. C. Pechmann, D. M. Cole, C. E. Johnson, J. E. Ebel, P. T. German, and J. W. Given (1980). Epicentral locations for the Homestead Valley earthquake sequence, March 15, 1979, *Calif. Div. Mines Geol. Calif. Geol.* **33,** 110–114.

Jennings, C. W. (1975). Fault map of California with locations of volcanos, thermal springs and thermal wells, 1:750,000, *Calif. Div. Mines Geol. Geologic Map No. 1.*

Johnson, C. E. and D. M. Hadley (1976). Tectonic implications of the Brawley earthquake swarm, Imperial Valley, California, January 1975, *Bull. Seism. Soc. Am.* **66,** 1133–1144.

King. N. E. and J. C. Savage (1984). Regional deformation near Palmdale, California, 1973–1983, *J. Geophys. Res.* **89,** 2471–2477.

Lee, W. H. K. and J. C. Lahr (1975). HYPO71 (revised): a computer program for determining hypocenter, magnitude, and first motion pattern of local earthquakes, *U.S. Geol. Surv., Open-File Rept. 75-311,* 133 pp.

Lee, W. H. K., R. F. Yerkes, and M. Simirenko (1979). Recent earthquake activity and focal mechanisms in the Western Transverse Ranges, California, *U.S. Geol Surv. Cir. 799-A,* 1–26.

McKenzie, D. P. (1969). The relation between fault plane solutions for earthquakes and the directions of the principal stresses, *Bull. Seism. Soc. Am.* **59,** 591–601.

Nicholson, C., P. Williams, L. Seeber and L. Sykes (1983). San Andreas seismicity and fault tectonics through the Eastern Transverse Ranges (abstract), *EOS* **64,** 768.

Oliver, H. W. (1980). Interpretation of the gravity map of California, *Calif. Div. Mines Geol. Bull. 205,* 1–8.

Pechmann, J. C. (1983). The relationship of small earthquakes to strain accumulation along major faults in Southern California, *Ph.D. Thesis,* California Institute of Technology, Pasadena, California.

Rasmussen, G. S. (1981). San Andreas fault geometry and maximum probable earthquakes in Southern California (abstract), *Geol Soc. Am. Abstr. with Prog.* **13,** 102.

Sanders, C. O. and H. Kanamori (1984). A seismotectonic analysis of the Anza seismic gap, San Jacinto

Fault Zone, Southern California, *J. Geophys. Res.* **89,** 5873–5890.

Savage, J. C. (1983). Strain accumulation in western United States, *Ann. Rev. Earth Planet. Sci.* **11,** 11–43.

Sharp, R. V. (1981). Variable rates of Late Quaternary strike slip on the San Jacinto fault zone, southern Californa, *J. Geophys. Res.* **86,** 1754–1762.

Sibson, R. H. (1983). Continental fault structure and the shallow earthquake source, *J. Geol. Soc. London* **140,** 741–767.

Sieh, K. E. (1978). Slip along the San Andreas fault associated with the great 1857 earthquake, *Bull. Seism. Soc. Am.* **68,** 1421–1448.

Stein, R. S. and W. Thatcher (1981). Seismic and aseismic deformation associated with the 1952 Kern County, California, earthquake and relationship to the Quarternary history of the White Wolf fault, *J. Geophys. Res.* **86,** 4913–4928.

Stein, R. S. and M. Lisowki (1983). The 1979 Homestead Valley earthquake sequence, California: control of aftershocks and postseismic deformation, *J. Geophys. Res.* **88,** 6477–6490.

Stierman, D. J. and W. L. Ellsworth (1976). Aftershocks of the February 21, 1973 Point Mugu, California earthquake, *Bull. Seism. Soc. Am.* **66,** 1931–1952.

Vetter, U. R. and A. S. Ryall (1983). Systematic change of focal mechanism with depth in the Western Great Basin, *J. Geophys. Res.* **88,** 8237–8250.

Whitcomb, J. H. (1973). The 1971 San Fernando Earthquake series focal mechansms and tectonics, *Ph.D. Thesis* (Part II), California Institute of Technology, Pasadena, California.

Yeats, R. S. (1981). Quaternary flake tectonics of the California Transverse Ranges, *Geology* **9,** 16–20.

SEISMOLOGICAL LABORATORY
CALIFORNIA INSTITUTE OF TECHNOLOGY
PASADENA, CALIFORNIA 91125 (H.K.)
CONTRIBUTION NO. 4131

GEOPHYSICS DIVISION
D.S.I.R.
P.O. Box 1320
WELLINGTON, NEW ZEALAND (T.W.)

Manuscript received 28 August 1984

APPENDIX

The table is a listing of events discussed in this study. Events 1 to 57 are from this work while events 58 to 69 are from other sources given in the text.

No.	Date	Time	North Latitude (deg	min)	West Longitude (deg	min)	Z (km)	M_L	Dip 1	Rake 1	Strike 1	Dip 2	Rake 2	Strike 2
1A	740119	1313	36.77	34	21.94	117	2.81	4.7	3.8	80.0	−159.6	− 74.0	69.9	−10.7	−167.7
1B	740119	1313	36.77	34	21.94	117	2.16	5.5	3.8	75.0	−169.6	− 81.0	80.0	−15.2	−173.7
2	750130	1403	18.13	33	59.95	116	44.95	10.0	3.2	18.1	−98.2	83.2	72.1	−87.3	271.8
3	750814	0808	50.00	34	2.43	116	26.33	7.4	4.0	52.0	−164.7	136.0	78.0	−39.0	36.4
4	751021	0915	52.00	33	57.79	116	24.40	9.3	3.7	74.0	−161.2	164.0	72.0	16.8	68.6
5	760229	2230	09.75	34	8.83	116	43.11	3.3	3.8	84.0	−175.0	133.0	85.0	−6.0	42.5
6	760417	0416	20.36	33	59.98	116	43.37	13.7	3.0	77.9	162.5	292.3	72.9	12.7	26.1
7	770210	1210	47.61	33	58.35	116	34.60	7.8	3.6	80.0	157.6	−42.0	67.9	10.8	52.1
8	770713	0812	48.51	33	59.98	116	49.73	10.7	3.1	64.0	153.2	−81.0	66.1	28.6	21.5
9	770922	0941	10.52	33	58.61	116	34.89	8.1	3.5	69.0	148.5	−48.0	60.8	24.2	54.4
10	771022	0459	17.35	34	23.17	117	2.95	3.9	3.7	90.0	180.0	129.0	90.0	0.0	39.0
11	771226	1836	08.21	33	59.71	116	50.82	10.4	3.3	90.0	180.0	316.0	90.0	0.0	46.0
12	780205	0953	40.99	34	18.70	116	43.00	0.6	3.7	40.0	−107.1	164.0	52.1	−76.1	5.9
13A	780206	0039	25.63	34	2.16	116	46.62	14.5	3.1	75.0	14.5	48.0	76.0	164.5	−45.8
13B	780206	0039	25.63	34	2.23	116	46.55	15.1	3.1	74.0	157.0	−50.0	67.9	17.3	46.7
14A	780206	0101	28.71	34	2.07	116	46.72	14.9	3.3	90.0	166.0	124.0	76.0	0.0	−146.0
14B	780206	0101	28.70	34	2.07	116	46.76	15.5	3.3	62.0	11.4	46.0	80.0	151.5	−49.4
15	780401	1052	27.27	34	11.84	116	57.97	10.6	4.0	62.0	−158.4	−29.0	71.0	−29.8	−129.5
16	780425	2206	32.06	33	59.14	116	56.06	21.0	3.3	64.0	−110.6	−158.0	32.7	−54.2	62.6
17	780429	0403	46.02	34	13.71	116	33.68	9.2	3.8	58.0	−151.4	182.0	66.0	−35.5	75.9
18	780616	0421	31.88	35	1.16	119	7.62	2.8	4.3	52.0	101.2	90.0	39.4	76.1	−107.8

No.	Date	Time	North Latitude (deg min)	West Longitude (deg min)	Z (km)	M_L	Dip 1	Rake 1	Strike 1	Dip 2	Rake 2	Strike 2
19	780726	0038 53.53	34 21.19	116 54.62	8.3	3.7	74.0	134.9	121.0	47.1	22.1	−133.5
20	780811	0047 30.31	34 9.50	117 26.65	6.7	3.9	80.0	169.8	310.0	80.0	10.2	41.8
21	781120	0655 09.27	34 9.03	116 58.42	12.8	4.3	84.0	−154.8	−29.0	65.0	−6.6	−121.8
22	781201	2320 46.38	33 55.83	116 40.68	13.8	3.6	63.0	−166.5	−25.0	78.0	−27.7	−121.2
23	790101	2038 18.01	34 55.89	119 9.70	0.0	3.2	78.0	83.4	299.0	13.7	118.5	148.2
24	790101	2322 14.19	33 55.95	118 42.84	13.0	3.4	22.0	46.3	−27.0	74.3	105.6	−161.1
25	790103	1336 50.45	34 55.90	119 9.71	1.2	3.5	80.0	90.0	270.0	10.0	90.0	90.0
26	790103	2000 42.66	35 1.81	119 9.26	5.7	3.4	28.0	131.3	128.0	69.4	70.6	−96.9
27	790121	1611 35.97	34 39.47	117 44.51	8.1	3.1	20.0	116.3	44.0	72.1	80.8	108.3
28A	790311	0714 05.03	34 1.00	116 43.49	14.5	3.4	26.0	−90.0	40.0	64.0	−90.0	−140.0
28B	790311	0714 05.01	34 1.07	116 43.64	15.8	3.4	85.0	−90.0	−138.0	5.0	−90.0	42.0
29A	790318	2253 02.68	34 13.84	116 21.70	4.6	4.2	88.0	−162.0	152.0	72.0	−2.0	61.3
29B	790318	2253 02.68	34 13.84	116 21.70	5.1	4.2	88.5	14.8	56.2	75.2	178.4	−34.2
30	790331	0016 08.58	34 18.33	116 29.96	1.3	4.2	80.0	−159.7	173.0	70.0	−10.6	79.3
31	790520	1204 47.80	34 5.43	116 22.64	2.5	3.7	90.0	−170.0	157.0	80.0	0.0	67.0
32	790629	0553 20.31	34 14.79	116 53.89	9.4	4.6	54.0	−134.0	−42.0	54.4	−46.3	−163.4
33	790630	0034 11.48	34 14.71	116 53.49	9.8	4.9	85.0	151.9	112.0	62.0	5.7	−155.3
34	790630	0703 52.81	34 14.97	116 53.76	9.8	4.5	80.0	−147.4	−76.0	57.9	−11.8	−172.3
35A	790713	0226 03.37	34 15.56	116 26.25	4.5	4.0	60.0	−180.0	146.0	90.0	−30.0	56.0
35B	790713	0226 03.37	34 15.56	116 26.25	5.1	4.0	52.0	−164.7	157.0	78.0	−39.0	57.4
36	790713	0351 23.46	34 15.38	116 26.37	6.6	3.9	70.0	−137.8	157.0	50.9	−26.2	49.8
37	791018	0425 42.92	33 55.91	118 40.58	12.8	3.0	75.0	92.8	−83.0	15.2	79.8	86.5
38A	791019	1222 37.69	34 12.58	117 31.70	4.8	4.1	90.0	−154.0	125.0	64.0	0.0	35.0
38B	791019	1222 37.69	34 12.54	117 31.72	5.5	4.1	65.0	176.7	126.0	87.0	25.0	−142.6
39	791207	2354 36.37	34 0.64	116 42.92	17.6	3.3	88.0	154.0	−48.0	64.0	2.2	43.0
40	800216	0145 15.16	34 16.98	119 37.27	11.3	3.1	20.0	99.3	−83.0	70.3	86.6	87.1
41A	800310	0654 21.93	33 53.63	116 16.79	4.7	3.7	84.0	−2.0	167.0	88.0	−174.0	−102.8
41B	800310	0654 21.94	33 53.59	116 16.97	5.5	3.7	85.0	−15.1	73.0	75.0	−174.8	164.3
42	810912	2124 07.36	34 9.79	117 16.03	4.0	3.6	45.0	−131.3	−31.0	57.9	−56.6	−159.8
43	810925	1413 38.04	34 0.99	116 50.79	20.0	3.3	50.0	−153.3	−29.0	69.9	−43.2	−136.9
44	811110	0029 44.40	35 1.33	119 8.16	3.1	4.5	44.0	87.1	73.0	46.1	92.8	−103.0
45	811111	0029 44.40	35 0.95	119 9.89	2.4	3.4	70.0	80.3	58.0	22.1	114.7	−95.5
46	811116	1201 45.21	35 1.54	119 8.72	1.7	3.2	60.0	79.4	72.0	31.7	107.7	−87.5
47	811224	0223 07.70	34 0.58	116 46.36	18.9	3.3	76.0	31.1	−5.0	60.0	163.8	−103.3
48	820225	0519 42.22	34 6.73	116 23.49	4.0	3.8	63.0	−141.3	169.0	56.2	−33.1	59.0
49	820609	0328 09.11	33 56.88	116 53.25	16.0	3.2	84.0	152.8	−55.0	63.0	6.7	38.1
50	820707	0844 33.50	34 9.11	116 42.00	13.8	3.6	86.0	−168.0	131.0	78.0	−4.1	40.1
51	821110	1121 25.64	34 3.37	116 40.16	9.2	3.6	70.0	−164.0	−61.0	75.0	−20.7	−156.6
52	830108	2251 30.35	34 8.14	117 27.10	7.7	4.1	80.0	−153.6	127.0	64.0	−11.1	32.1
53A	830912	1208 02.72	34 3.06	117 15.16	14.5	3.5	55.0	−2.4	63.0	88.0	−145.0	154.4
53B	830912	1208 02.71	34 2.94	117 15.25	15.5	3.5	42.0	0.0	61.0	90.0	132.0	−29.0
54	831007	1040 24.72	33 58.58	116 57.89	13.6	3.1	74.0	148.6	324.0	60.0	18.6	63.5
55	831023	2335 43.91	35 4.05	119 2.17	12.9	3.1	66.0	−89.2	26.0	24.0	−91.8	−156.0
56	831029	0638 02.50	33 59.77	116 36.51	12.0	3.4	76.0	10.3	20.0	80.0	165.8	−72.5
57A	840123	1703 16.05	33 58.11	116 50.60	14.9	3.1	46.6	−23.9	41.5	72.9	−134.0	148.4
57B	840123	1703 16.04	33 58.14	116 50.67	15.5	3.1	43.0	−22.0	42.8	75.2	−130.8	149.3
58	700416	2155 48.50	34 15.70	119 42.20	8.9	2.9	76.0	110.1	288.0	24.3	35.9	51.4
59	720117	0549 58.20	34 17.80	120 15.70	10.3	2.7	76.0	90.0	296.0	14.0	90.0	116.0
60	720714	2301 15.70	34 3.00	118 47.80	6.6	2.7	70.0	78.7	287.0	22.8	118.2	137.2
61	720727	0112 04.40	34 43.20	118 56.90	8.0	3.0	10.0	−151.1	24.0	85.2	−81.2	−94.5
62	730226	0650 39.70	34 4.89	118 59.94	15.3	2.7	90.0	90.0	155.0	0.0	90.0	−25.0
63	730301	1841 41.66	34 4.45	118 59.61	14.6	2.5	85.0	90.0	150.0	5.0	90.0	−30.0
64	730407	2100 28.35	34 6.08	118 58.68	13.0	1.7	80.0	90.0	140.0	10.0	90.0	−40.0
65	740425	0823 53.50	34 1.50	119 5.80	8.9	2.8	72.0	81.1	271.0	20.0	115.5	118.0
66	760408	1521 38.07	34 20.81	118 39.34	14.5	4.6	75.0	97.4	130.0	16.7	64.4	−76.6
67	761017	0538 11.87	34 27.16	118 22.26	11.2	3.9	85.0	93.2	−80.0	5.9	57.4	67.3
68	780814	0102 35.61	34 25.47	119 41.34	12.5	3.1	77.6	89.5	109.2	12.4	92.3	−68.4
69	780814	0701 19.21	34 25.89	119 43.50	7.6	2.5	82.0	88.4	90.1	8.2	101.2	−78.6

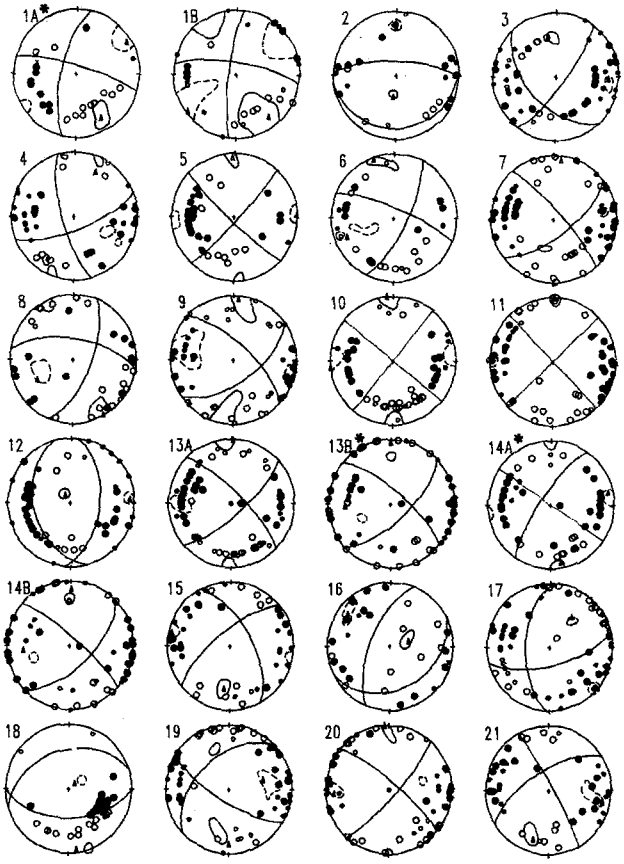

FIG. A1. Equal-area, lower hemisphere plots of all focal mechanism solutions obtained in this study. Solid circles indicate a compressional arrival. The meaning of the small symbols is discussed in the text. Triangles denote the positions of the P and T axes while the solid and dashed contours denote the locus of P and T axis positions, respectively, for which there are a minimum number of stations in error.

FIG. A2. Equal-area, lower hemisphere plots of all focal mechanisms solutions obtained in this study. Solid circles indicate a compressional arrival. The meaning of the small symbols is discussed in the text. Triangles denote the positions of the P and T axes while the solid and dashed contours denote the locus of P and T axis positions, respectively, for which there are a minimum number of stations in error.

FIG. A3. Equal-area, lower hemisphere plots of all focal mechanism solutions obtained in this study. Solid circles indicate a compressional arrival. The meaning of the small symbols is discussed in the text. Triangles denote the positions of the P and T axes while the solid and dashed contours denote the locus of P and T axis positions, respectively, for which there are a minimum number of stations in error.

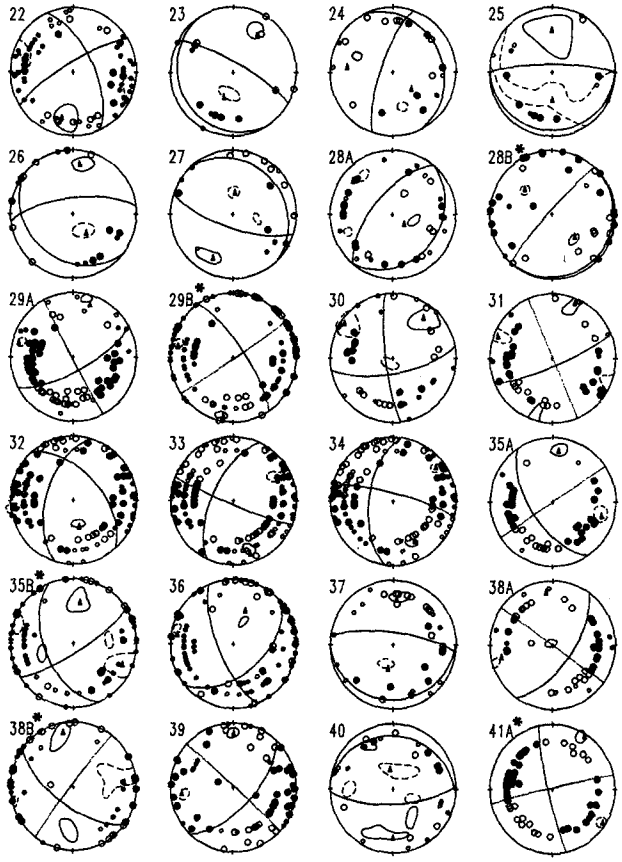
22
23
24
25
26
27
28A
28B*
29A
29B*
30
31
32
33
34
35A
35B*
36
37
38A
38B*
39
40
41A*

FIG. A2

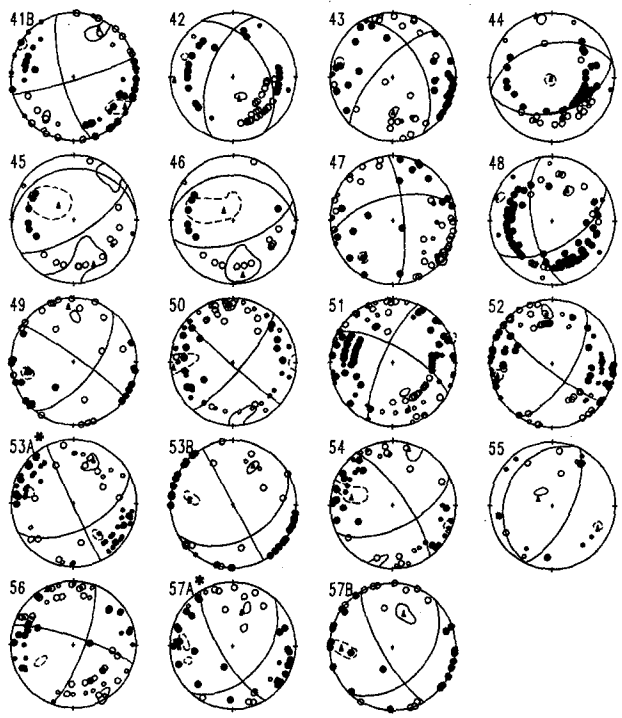
41B
42
43
44
45
46
47
48
49
50
51
52
53A*
53B
54
55
56
57A*
57B

FIG. A3